Applied Materials Today 29 (2022) 101657

Contents lists available at ScienceDirect

Applied Materials Today

journal homepage: www.elsevier.com/locate/apmt

Electrophoretic deposition of halloysite nanotubes/PVA composite coatings for corrosion protection of metals

Yao Wang [a], Yuer Yang [b], Mingxian Liu [a,*]

[a] Department of Materials Science and Engineering, College of Chemistry and Materials Science, Jinan University, Guangzhou 511443, China
[b] College of Cyber Security, Jinan University, Guangzhou 510632, China

ARTICLE INFO

Keywords:
Nanotube
Nanocomposites
Assembly
Coating
Corrosion

ABSTRACT

The application of nanotechnology in the corrosion protection of metals has gained considerable attention. In this work, a fast, low-cost, and facial method of metal protection was proposed by electrophoretic deposition (EPD) of halloysite nanotubes (HNTs). EPD is a standard method to prepare dense homogeneous polymers gaining wide application. HNTs exhibiting unique nanostructure, high surface potentials, and good dispersion ability were used as the different metals' coating materials. The coating thickness can be precisely controlled by changing the electrophoretic deposition conditions (time, concentration, electrode spacing, and voltage). Coatings of 50 μm thickness were achieved at conditions of deposition time of 30 s, HNTs concentration of 4%, electrode spacing of 30 mm, and voltage of 20 V. The HNTs coating can be applied to complex shapes and different metal types. To increase the water resistance, glutaraldehyde crosslinked polyvinyl alcohol (PVA) was further introduced to the coating. PVA modification increased the corrosion resistance, wear resistance, and water resistance. The surface roughness increased with the deposition time, as evidenced by SEM and 3D optical profiler. When the deposition time was increased from 15 to 60 s, the RMS roughness of the coatings increased from 1.46 to 2.82 μm. HNTs/PVA composite coatings on metals are used for thermal insulation, information hiding, and anti-corrosion. When the deposition time increased from 15 to 60 s, the coating resistance changed from 13,446.0 to 27,015.0 Ω cm^2. This work developed an assembled method of nanoclays on metals by EPD and polymer modification, which shows excellent potential in metal anti-corrosion.

1. Introduction

Metal materials damaged by the surrounding media, known as metal corrosion, involved multiphase reactions at the metal interface, which brought severe problems such as decreased strength, plasticity, toughness, and other mechanical properties [1]. Metals' anti-corrosion has become a priority to ensure safety, efficiency, and long-term durability and cut costs [2]. Metal corrosion protection is a systematic project, and the widely used corrosion protection techniques mainly contain the following four aspects, i.e., proper selection of material [3], surface protection [4–6], handling of corrosive media and electrochemical protection techniques. Surface protection technology is a simple and effective method using various coatings to provide a space barrier to the external corrosive environment. [7–9].

Electrophoretic deposition (EPD) is a desirable method to prepare protective coatings, which is also an approach for preparing composite film deposition for biomedical applications [10]. EPD technique has been widely used for the deposition of inorganic materials [11], polymers [12] and composites [13], which is highly cost-effective due to its simplicity [14]. It is possible to produce smooth coatings on various metal surfaces, and the thickness of the deposited film is varied by adjusting the conditions of EPD [15]. In addition, EPD has been used to manufacture nanostructured conductive polymer films because of its ability to produce uniform and dense conductive polymer film electrodes [16–19]. For example, Hwang et al. have prepared corrosion protection for metal surfaces by EPD based on graphene oxide modified with phenylenediamine [20]. Multi-walled carbon nanotubes were also deposited on stainless-steel substrates by EPD methods for heat extraction devices or tissue engineering scaffold applications [21].

Halloysite is a natural silicate clay, often called halloysite nanotubes (HNTs), due to their empty lumen structure. HNTs can be applied in various fields owing to their unique tubular properties, ample surface area, high dispersion, good biocompatibility, non-toxicity, and low cost [22–25]. For instance, HNTs and their composites have been widely

* Corresponding author.
E-mail address: liumx@jnu.edu.cn (M. Liu).

https://doi.org/10.1016/j.apmt.2022.101657
Received 2 July 2022; Received in revised form 21 September 2022; Accepted 9 October 2022
Available online 26 October 2022
2352-9407/© 2022 Elsevier Ltd. All rights reserved.

used in ceramics, polymer composite, catalyst, tissue engineering [26], drug delivery carriers, cosmetics, and other fields [27]. HNTs possess an inner layer composed of an aluminoxane (Al-OH) group and an outer silanol (Si-OH) group [28], with the chemical formula of $Al_2Si_2O_5(OH)_4{\cdot}nH_2O$ [29]. HNTs vary in outer and inner diameters between 30 and 70 nm and 15 and 20 nm, respectively, while the tube length is between 200 and 1500 nm [30]. HNTs have predominantly negatively charged surfaces [31]. Therefore, HNTs particles could move to an anode under an electric field. HNTs can be used as a material for EPD, and a dense and homogeneous coating composed of HNTs can be formed on the substrates. The EPD of HNTs has been proven to be applicable previously [32–39]. For example, Deen et al. prepared composite films of HNTs, hydroxyapatite (HA), and hyaluronic acid by EPD for biomedical implant applications [10]. HNTs/chitosan nanocomposite coatings with drug delivery function and antimicrobial activity were developed by Farrokhi-Rad et al. through EPD [40]. EPD of silane modified HNTs on glass fabrics can also be applied to improve the mechanical properties of epoxy composite materials [41]. Due to the hydrophilicity of HNTs, the HNTs coating cannot be used for long periods for metal protection in wet environments. Covalent grafting of organic compounds such as organosilanes and organophosphorus acids on the Al-OH and Si-OH groups on HNTs was evidenced as an effective method to improve the water resistance of the HNTs coating [42].

This paper prepared a HNTs/PVA composite coating with excellent water resistance and corrosion resistance by glutaraldehyde crosslinking. The superiority of its physical properties was verified by the water resistance test, scratch resistance test, and thermal conductivity test. The metal protection performance was verified by the electrochemical impedance spectrum and Tafel curve. It was also found that the transparency of the HNTs coating increase after wetting, which can be used in information hiding. The HNTs coating prepared by EPD can be applied in complex shapes and various metals, and a deposition pattern can obtain by a mask method during the EPD process. This study has shown a bright future in manufacturing HNTs-polymer composite coating on metals by EPD, which shows potential in metal anticorrosion.

2. Materials and methods

2.1. Materials

Halloysite nanotubes (HNTs) (mined from Yunnan Province, China) was supplied from Guangzhou Runwo Materials Technology Co., China. Polyvinyl alcohol (PVA, 1788 model) was purchased from Deli Group Co., Ltd, China. Glutaraldehyde and poly(sodium-p-styrenesulfonate) (PSS) were obtained from Sigma-Aldrich. The dyes (methylene blue and neutral red) were obtained from Chengdu Aikeda Chemical Reagent Co., Ltd., China. Ferric chloride (III) hexahydrate and sodium chloride were purchased from Tianjin fuchen chemical Co., Ltd, China. All the metal materials for EPD and ink were purchased from local markets.

2.2. Preparation of the HNTs/PVA composite coatings

2.2.1. Preparation of PSS-modified halloysite

HNTs were modified using PSS to improve the tubes' surface charge and dispersion stability [43]. HNTs powder and PSS were placed in a beaker at a mass ratio of 10:1. The addition of PSS made the Zeta potential of HNTs dispersion change from −24.2 to −29.2 mV. The mixture was stirred magnetically at room temperature for 48 h to allow specific adsorption. The mixture was then centrifuged in a centrifuge at 8000 rpm for 10 min. The supernatant was discarded, and the precipitation was washed three times with anhydrous ethanol, and then dried and ground into a powder to give modified HNTs powder.

2.2.2. EPD preparation of HNTs coatings

EPD of HNTs coating was conducted by the instrument of a two-way DC regulated power supply (APS3005S-3D, Shenzhen ATTEN Technology Co., Ltd, China) with the copper sheet as the positive and negative electrodes at a set voltage of 5–25 V and an electrodes distance of 10–40 mm. The concentration of HNTs aqueous dispersion varied from 1 to 4 wt.%, and the deposition time was 15–60 s. Electrophoretic deposition times that were too short can result in coatings that were too thin to cover the substrate (Fig. S1). Excessive deposition time could cause stress cracking on the coating surface during drying, which was not satisfactory for the corrosion protection application. After electrophoretic deposition, the positive copper sheet was dried at room temperature for at least 1 h until complete drying.

2.2.3. Preparation of HNTs/PVA composite coatings

A 5% PVA aqueous solution was used to immerse the completely dried HNTs coating. After the coating was completely wet, the coating was removed and dried naturally at room temperature. PVA could form a thin film on the surface of the HNTs coating. The HNTs/PVA composite coating was then immersed in a 5% GA aqueous solution and crosslinked in an oven at 60 °C for 1 h [44].

2.3. Characterization

The elemental composition of HNTs was determined by X-ray fluorescence (XRF) (Malvern Panalytical, United Kingdom). Field emission scanning electron microscopy (SEM, ULTRA55, Carl Zeiss Jena, Germany) was used to analyze the morphology of the HNTs coating. Before testing, a layer of gold was sprayed on the coating surfaces. Energy dispersive spectrometry (EDS) mapping were also employed to explore the element distribution. Fourier transforms infrared (FTIR) spectra were obtained with a Thermo FTIR (Nicolet iS50, Thermo Fisher Scientific Co. Ltd., USA) spectrometer. X-ray diffraction (XRD) patterns were recorded with Cu Kα radiation using a Miniflex 600 diffractometer from RIKEN, Japan. TGA curves were obtained using a TGA instrument (TGA2, METTLER TOLEDO Ltd., Switzerland) and measured from 50 to 800 °C at a 50 mL/min nitrogen flow rate and a heating rate of 10 °C/min. 3D optical profiler (UP-DUAL MODE, Rtec Instrument Ltd., USA) was used to study the surface morphology. The 3D morphology was analyzed by Gwyddion analysis software to obtain linear profiles.

2.4. Water resistance and abrasion resistance test

2.4.1. Contact angle tester

Water contact angle (WCA) was tested at room temperature using a contact angle tester (DSA100, Kruss Ltd, Germany). The water contact angle image was captured immediately after the release of water droplets. The volume of the water droplets was 10.0 ± 0.5 μL. At least five measurements were made per substrate.

2.4.2. Simulated rain washout test

The coatings were placed in a Petri dish to investigate the water resistance. An appropriate amount of water was drawn from a syringe without a needle and injected onto the surface of the coatings at a specific rate and allowed to wet well to observe whether the coatings peeled off or showed deformation. Then, the water was poured out of the Petri dish, and the coating surface was dried with a hairdryer and compared with the coating before immersion in water.

2.4.3. Abrasion resistance test

The coatings of HNTs before and after treated by PVA and GA were applied with a 100 g load and sandpaper and pulled in a vertical direction for 10 cm. The appearances were observed by the photograph. Furthermore, for more visual and quantitative analysis, the weight changed of the coatings after 9 times abrasion were recorded by an electronic balance.

2.5. EPD of HNTs on different substrates

Experiments were designed to perform the EPD of HNTs on different metal substrates with complex shapes. Copper foam, nickel foam, screw nuts, key fobs, or other decorative objects were used as experimental materials to observe the electrophoretic deposition of HNTs.

2.6. Preparation of specific patterns of HNTs coatings

To verify that EPD can prepare a specific pattern of HNTs coatings. A non-conductive material was used as a mask to cover part of the coating during the EPD process, allowing HNTs to be deposited on the exposed part. The deposited coating was dried in an oven, and the mask was carefully removed to obtain a specific pattern of HNTs coatings after complete drying.

2.7. Thermal conductivity test

The thermal conductivity studies were firstly investigated by measuring water temperature on an HNTs coated copper substrate. HNTs coatings with deposition time of 1, 2, and 3 min were selected to test their thermal conductivity (at a voltage of 20 V, a distance of 30 mm between the poles, and a dispersion concentration of 4%). The heating plate temperature was set at 70 °C, and a small bottle containing 20 mL of water was placed on the heated plate. The water temperature was measured by an infrared thermal imager (TiS 55, Fluke Electronic Instrument Ltd., USA). The melting of the wax on the HNTs coating and the copper plate was then compared. The copper sheet with and without HNTs coating was placed on a heating plate at 150 °C, and two bottles of wax were placed on the metal sheets.

2.8. Corrosion resistance testing

To investigate the corrosion behavior of HNTs/PVA composite coatings, polarization tests and electrochemical impedance spectroscopy (Shanghai Chenhua CHI760E) were carried out at room temperature, using graphite and standard glycine electrodes (SCE) as auxiliary electrodes. For the reference electrode, impedance spectra were obtained in the frequency range of 10 MHz to 30 MHz, respectively, with an amplitude of 20 mV.

Copper was used as the metal model. A ferric chloride solution was obtained by adding 0.75 g of initially ground ferric chloride powder to 0.6 mL of concentrated hydrochloric acid and 0.9 mL of water, followed by a slow dilution to 30 mL with water. Composite coatings of HNTs/

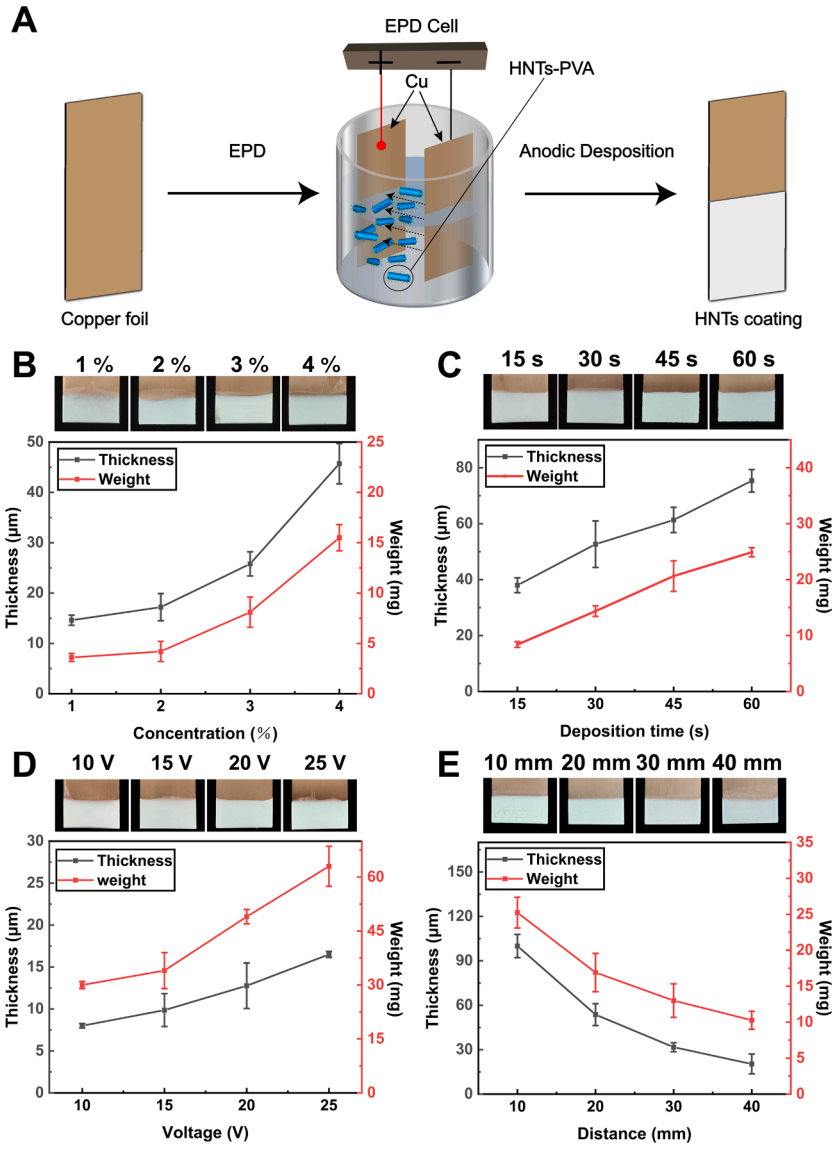

Fig. 1. Schematic showing the EPD process of HNTs coating (A). The influence of HNTs concentration (at a voltage of 20 V, electrode spacing of 30 mm and deposition time of 30 s) (B), deposition time (at a voltage of 20 V, an electrode spacing of 30 mm and a concentration of 4%) (C), voltage (at an electrode spacing of 30 mm, a deposition time of 30 s, and a concentration of 4%) (D), and electrode spacing(at a voltage of 20 V, a deposition time of 30 s and a concentration of 4%) (E) on the coating thickness and weight.

PVA with a deposition time of 15–60 s were prepared on copper rods by EPD. The composite coating and copper rods were placed in the ferric chloride solution for 48 h, and the corrosion of each sample was observed.

3. Results and discussion

3.1. Factors affecting the EPD of HNTs

Clays always have a net negative charge because silica (Si^{4+}) is substituted by aluminum (Al^{3+}) in the mineral structure. This replacement leads to negative charged surfaces of HNTs [45]. However, the negative charges of raw HNTs are not enough for stable dispersion in an aqueous medium. PSS was added to improve the negative charge and the uniform dispersion of the HNTs suspension [46]. The purities of HNTs may have an influence on the EPD process and the coating appearances. The elemental composition by XRF of the used HNTs was determined as follows (wt%): SiO_2, 53.26; Al_2O_3, 44.98; Fe_2O_3, 0.35; P_2O_5, 0.75; CaO, 0.36. The purity of HNTs was 98.24% which was calculated by the sum of the content of SiO_2 and Al_2O_3. Fig. 1**A** shows the schematic for preparing HNTs coating by the EPD method.

To study the factors affecting EPD, HNTs concentration, deposition time, voltage, and the distance between the two poles were changed, and the thickness and weight of the coating were recorded. The coating thickness was tested by a calibrator, while a balance tested the coating weight.

Fig. 1**B** shows the influence of HNTs concentration on the coating thickness and weight. The thickness of HNTs coating at a concentration of 4% (45.7 μm) is approximately three times the thickness of 1% (14.6 μm), and the average deposition weight increased from 3.6 mg to 15.5 mg. Fig. 1**C** shows that the coating thickness with a deposition time of 60 s (75.3 μm) is approximate twice the coating thickness with a deposition time of 15 s (38.0 μm). The coating weight increases with deposition time from 8.4 mg to 24.9 mg. Fig. 1**D** shows the relationship

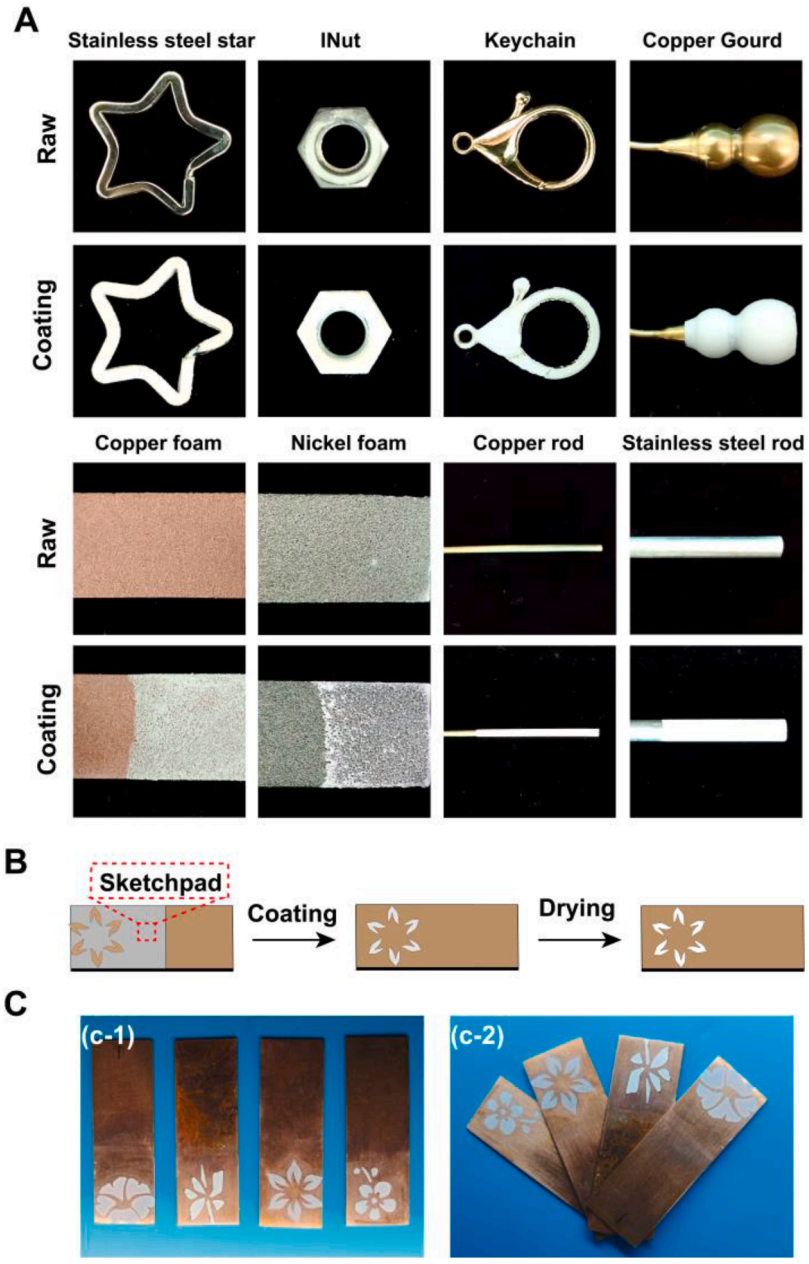

Fig. 2. EPD of HNTs on various substrates (A). A specific shape of patterned HNTs coatings prepared by mask (B); Appearance of patterned HNTs coatings on copper substrate (C).

between the thickness and weight of the coating with voltage. The thickness increases from 30.0 μm to 63.0 μm when the voltage varies from 10 V to 25 V, and average weight increased from 8.0 mg to 16.5 mg. Electrode spacing also affects the coating thickness. The farther the spacing, the less deposition. 10 mm electrode spacing resulted in 100.0 μm thickness and 10.3 mg average weight, while 40.0 mm electrode spacing resulted in 20.3 μm thickness and 25.2 mg average weight (Fig. 1**E**). Therefore, increasing the HNTs concentration, deposition time, and voltage leads to a regular increase in the thickness and weight of the EPD coating. Increasing the distance between the two electrode plates will lead to a regular decrease in the thickness and weight of the EPD coating. It should be noticed that the HNTs coating will become uneven, and cracks occur if further increasing the concentration and deposition time, and voltage.

3.2. EPD of HNTs on different substrates and patterned HNTs coating

Copper is a suitable substrate for the EPD of HNTs due to its good conductivity and proper surface roughness. A further experiment is needed on whether HNTs can be deposited into other metals by EPD. Several commonly used metal materials were selected for the EPD of HNTs, such as keychains, nuts, copper artifacts, copper rods, stainless steel bars, and foam metals. Due to the different conductivity of each material, EPD conditions were varied to prepare a uniform coating of HNTs. The appearances of these objects before and after the EPD of HNTs coating are shown in Fig. 2**A**. HNTs can form uniform coatings on the surfaces of these metal objects. It should be noted that the EPD coating can only be formed on one side of the object if the object is static. Uniform coating on these 3D objects can be obtained by rotating these objects at a reasonable rate.

To meet the different shapes requirement of HNTs coating on metals, a mask with a special pattern was adhered to the metal surface before EPD, and the mask was removed after EPD (Fig. 2**B**). Four different flower-shaped HNTs coatings are successfully prepared on copper surface, giving the coatings an aesthetically pleasing appearance (Fig. 2**C**). These results show that HNTs can be prepared in complex shapes by covering part of the conductive material during the EPD process, which shows applications in designation such as product logos. HNTs coating can also be deposited onto various conductive metals using EPD technology, which makes the HNTs coating application in medical metal implant, metal protection, and thermal insulation for metals.

3.3. Surface studies of HNTs/PVA composite coatings

GA crosslinked PVA was further introduced on the HNTs coating to increase the water resistance. The surface morphology of HNTs/PVA composite coatings with different EPD time was investigated by FE-SEM. HNTs were irregularly arranged on the surface of the coating, and the arrangement pattern of HNTs did not change significantly as the thickness of the coating increased (Fig. 3**A**). The surface of GA crosslinked HNTs/PVA coating is rough and porous. PVA can form a thin film on the HNTs coating, but the film is broken by GA crosslinking. This suggests that GA can interact with PVA and HNTs since hydrogel groups on them can react with aldehyde groups of GA. Besides, PVA and HNTs can interact via hydrogen bonding [47]. In addition, the distribution of HNTs in the PVA coating was uniform , as shown by EDS results in Fig. S2.

The coating thickness affected the surface roughness of HNTs/PVA (Fig. 3**B**). As the deposition time increased from 15 to 60 s, the distance between the highest and lowest points of the coating increased from 11.6 μm to 16.6 μm. The RMS roughness of the coating was 1.46, 1.65, 2.13, and 2.82 μm for a deposition time of 15, 30, 45, and 60 s, respectively. Thus, the RMS roughness of the HNTs/PVA composite coating increased with increasing coating thickness. Fig. 3**C** shows the

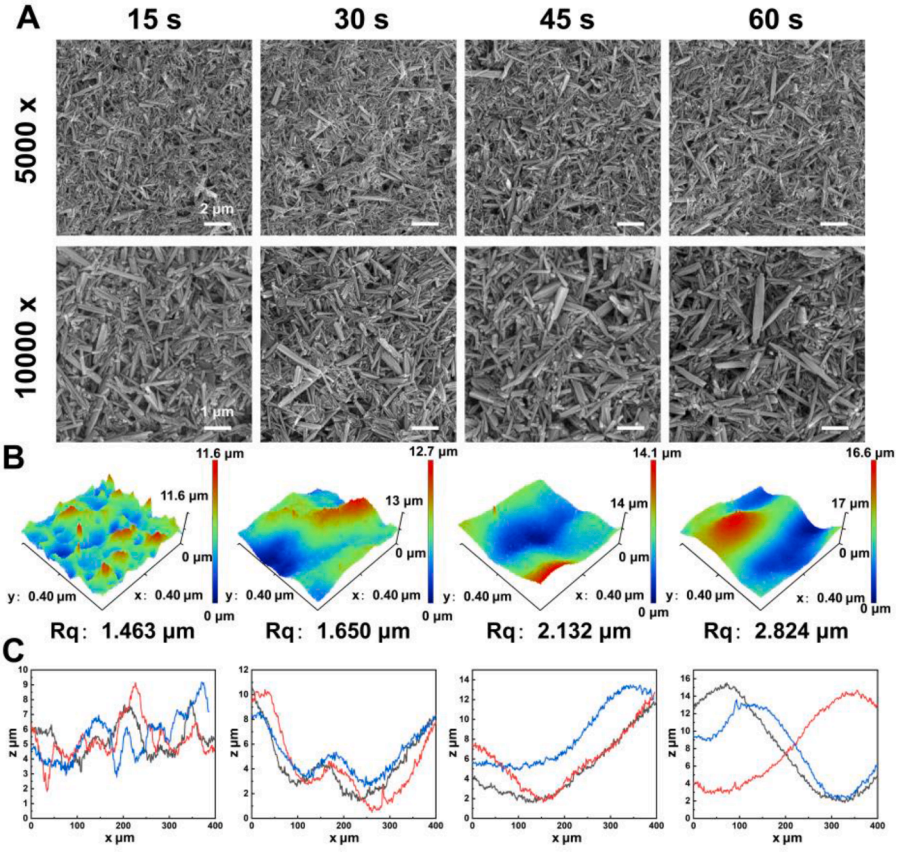

Fig. 3. SEM images (A), 3D morphology (B), and surface height profiles (C) of HNTs/PVA coatings with deposition times of 15–60 s.

height profiles in 3B. Similarly, the distance from peak to valley increases with the coating thickness. So, the surface roughness of the coating can be tailored by changing the deposition time.

XRD and FTIR spectra were used to investigate the structure of the EPD coatings. The positions and sizes of the characteristic diffraction peaks of HNTs in PVA and GA crosslinked PVA coating did not change, as shown in Fig. 4**A**. The peaks at 43, 52, and 74^{o} in the three curves are attributed to the (111), (200), and (220) planes of Cu. The higher the crystallinity, the stronger the peak intensity. The peak strength and position of HNTs and Cu do not change, so PVA and GA have almost no effect on the crystallinity of the HNTs and Cu. FT-IR technique was also used to characterize the structural changes of HNT (Fig. 4**B**). HNT shows typical absorption peaks around 3698, 3623, 1024, and 908 cm^{-1} assigned to O—H stretching of inner surface hydroxyl groups, O—H stretching of internal hydroxyl groups, in-plane Si-O stretching, and H deformation of O-internal hydroxyl groups, respectively [48]; PVA shows typical absorption peaks around 2928, 1650 cm^{-1} show typical absorption peaks assigned to saturated C—H stretching motion and C = O stretching motion, respectively. The peaks around 3698, 3623,1024, and 911 cm^{-1} of HNTs shift slightly in HNTs/PVA sample. So, it suggests there are hydrogen bonding interactions between HNTs and PVA.

The thermal stability of HNTs before and after modification with PVA and GA was compared by TGA (Fig. 4**C**). As seen from the TG and DTG curves, the maximum weight loss of HNTs started around 450 °C, which is due to the hydroxyl dehydration. The weight loss at 800 °C of HNTs and HNTs/PVA samples was 16.2% and 18.0%, respectively. The increased weight loss of the sample is attributed to the decomposition of the polymer chains. From TGA result, the PVA ratio in HNTs/PVA was calculated as 1.8 wt.%.

3.4. Scratch and water resistance

High-performance nanocoating requires good durability and strength; wear resistance is crucial. To compare the metal protection capability of HNTs/PVA composite coatings, the mechanical stability and coating adhesion of the HNTs before and after the introduction of PVA was tested by wear tests. The coating of HNTs and HNTs/PVA was placed between a 100 g load and sandpaper and pulled vertically for 10 cm. This process was repeated nine times to observe the degree of wear on the coating surface, and the remaining coating weight was recorded [49]. Fig. 5A shows the appearance of two coatings after wear. The results show that HNTs coating exhibits severe surface damage, while the HNTs/PVA composite coating leaves only slight traces on the sandpaper, and surface wear is not significant. Fig. 5D shows that the HNTs/PVA coating lost only 10% of its weight after nine times of friction, while the HNTs coating lost almost 50% of its weight. Therefore, the HNTs/PVA composite coating provides good protection against frictional damage on the metal surface.

The water resistance of HNTs/PVA composite coatings is critical to their ability to protect metals in a wet environment. HNTs are typically hydrophilic materials with many hydrophilic groups on their surfaces [50]. Therefore, resistance to humid environments will be challenging when HNTs are used directly for corrosion protection in natural environments. The environment of rainwater washing over the coating was simulated (Fig. 5**B**). A syringe was used to rapidly inject water into the surface of the HNTs coating and the HNTs/PVA composite coating. After rinsing with water, the HNTs/PVA composite coating was intact, while the HNTs coating was almost completely peeled off. The water contact angle of the composites was then measured to compare the hydrophilicity of the material surface [51,52]. As shown in Fig. 5**C**, the highly hydrophilic (27.7°) HNTs coating became hydrophobic (88.2°) after the introduction of GA crosslinking of PVA.

The reason why PVA and GA can change the water repellency of the coating by crosslinking is that the crosslinking mechanism between PVA and GA involves a chemical bond between the hydroxyl groups present in PVA and the aldehyde group of GA, which usually occurs through the formation of -C-O-C- between the -OH of the typical PVA structure and the aldehyde groups of the GA molecule [53]. The GA crosslinking treatment resulted in a significant increase in its water resistance. This result indicates that the HNTs/PVA composite coating has good water resistance and can protect metals in wet environments. Therefore, the HNTs coatings prepared by EPD and treated by GA crosslinked PVA have

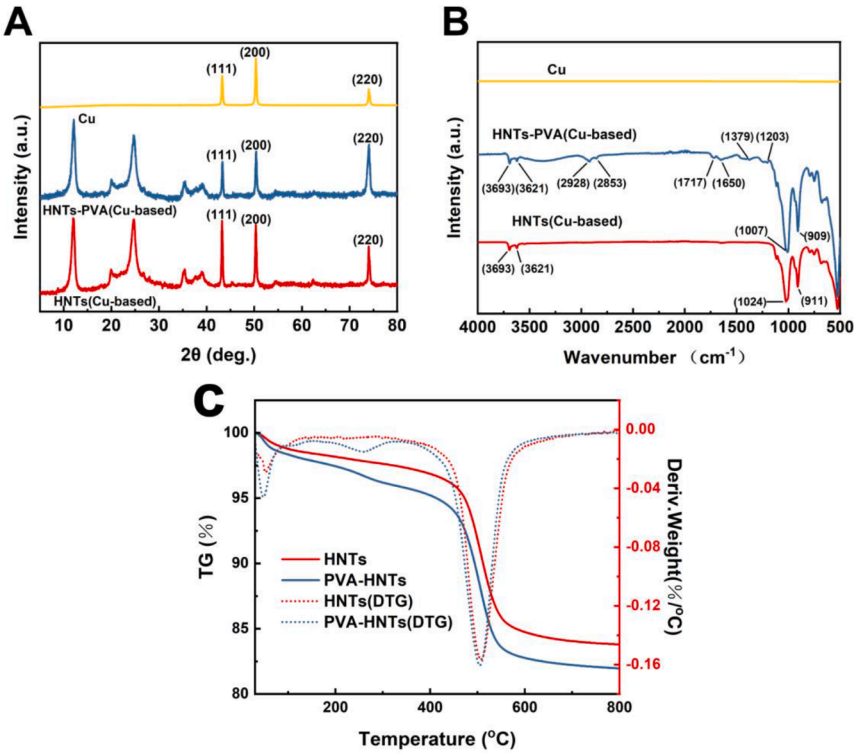

Fig. 4. Characterization of HNTs coating before and after modification by PVA and GA: XRD (A); FTIR (B); TG and DTG curves (C).

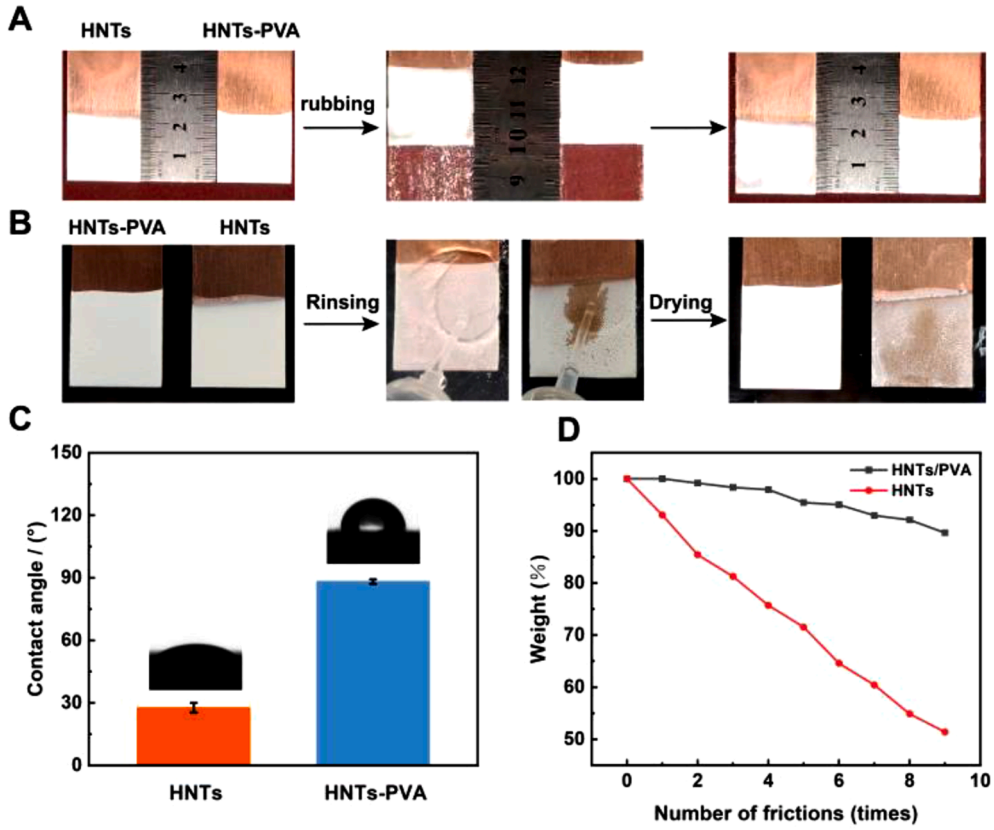

Fig. 5. Scratch resistance (A) and water resistance (B) testing of HNTs/PVA composite coatings and HNTs coatings; water resistance test of HNTs/PVA composite coating and HNTs coating (C); Plot of the number of coating rubs and the percentage of weight remaining (D).

good water and wear resistance, which has wide applications in metal protection.

3.5. Thermal conductivity test

The thermal conductivity of the HNTs/PVA composite coating is also an issue when applying this coating as thermally conductive material such as a pot. Two thermal conductivity studies were investigated to compare the influence of coating thicknesses on thermal conductivity by measuring the temperature of the water in a bottle placed on the coating with a heating plate (Fig. 6**A**) and by studying the melting process of the wax on the HNTs/PVA coating and the copper sheet. Fig. 6**B** shows that the water temperature starts to stabilize at approximately the 45th minute for all the samples. The final water temperature on the copper sheet was approximately 47.7 °C, and the final water temperature on the coating with a deposition time of 1, 2, and 3 min was approximately 46.6, 44.1, and 43.4 °C, respectively. Therefore, the final temperature of the water on the coating with a deposition time of 1 min was lower than the temperature of the water on the copper sheet, suggesting the decreased thermal conductivity property of the composite coatings.

Fig. 6C shows the appearance of wax placed on the copper sheet and the HNTs/PVA coatings. The wax first started to melt in a shorter period, starting at around 30 s and completely melting at 700 s for the copper sheet. In contrast, the wax on the composite coating took longer to melt, starting at around 70 s and completely melting at 720 s. The melting ratio of these two groups is compared in Fig. 6D. The results also show that the wax temperature on the copper sheet is higher than that on the HNTs/PVA coating. Therefore, HNTs/PVA composite coatings have improved thermal insulation properties. The thicker the coating, the better the thermal insulation property.

3.6. Applications in information hiding

During the preparation process of HNTs coating with EPD, it is found that the transparency of the coating increased significantly when the HNTs coating with a thickness more significant than 50 μm is in wet conditions. Interestingly, the transparency decreases when the coating is dried and becomes pure white. So, exploring whether HNTs coating can be applied to information hiding is one of the directions of this work.

Fig. 7A shows the information hiding process by the HNTs/PVA coating. Some text is written by ink on each of the three copper plates, and then the text is covered with HNTs/PVA coating by EPD. These coatings were colored with methylene blue and neutral red to enhance the readability of the coatings. The crosslinking of GA and PVA increased the coatings' water resistance while retaining the HNTs coatings' transparency. When exposed to water, the introduction of the GA crosslinked PVA allowed them to be repeatedly wetted and dried while maintaining the functionality and integrity of the coatings. The prepared HNTs coating was wetted with water to observe whether the text on the surface of the copper sheet could be visible through the coating.

The results are shown in Fig. 7**B**. When the HNTs coating is wet, the text on the copper sheet is visible through the coating. When the coating dries, the text on the copper sheet becomes invisible. By drying and wetting, the information can be effectively hidden and displayed. This process can be repeated at least ten times. Therefore, HNTs/PVA composite coating can be used for information hiding, which has excellent potential for security applications.

3.7. Applications in metal protection

The protection of the metal from corrosion of the HNTs/PVA composite coating is then tested. A corrosion etching experiment was

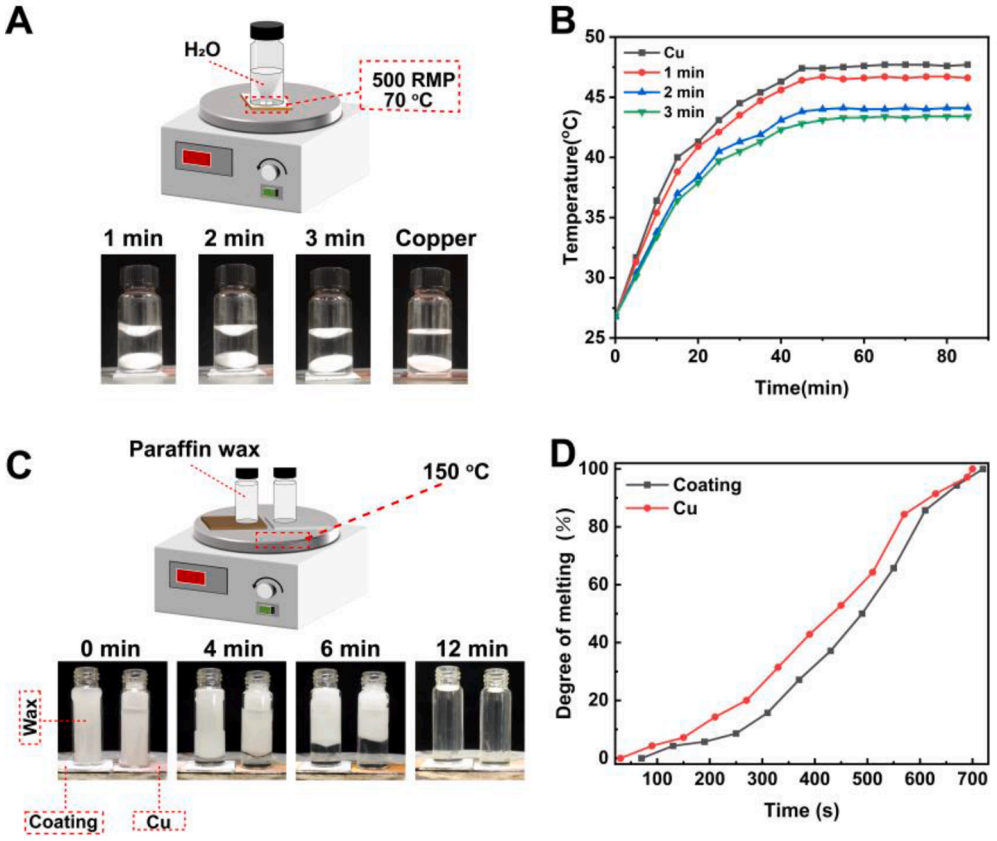

Fig. 6. Thermal conductivity study of HNTs/PVA composite coatings. Schematic showing of thermal conductivity tests on HNTs/PVA composite coatings and copper sheets with deposition times ranging from 1 min to 3 min (A); water temperature on different thicknesses of coatings (B); the schematic showing the wax melting experiments (C); melting percentage of paraffin wax with time (D).

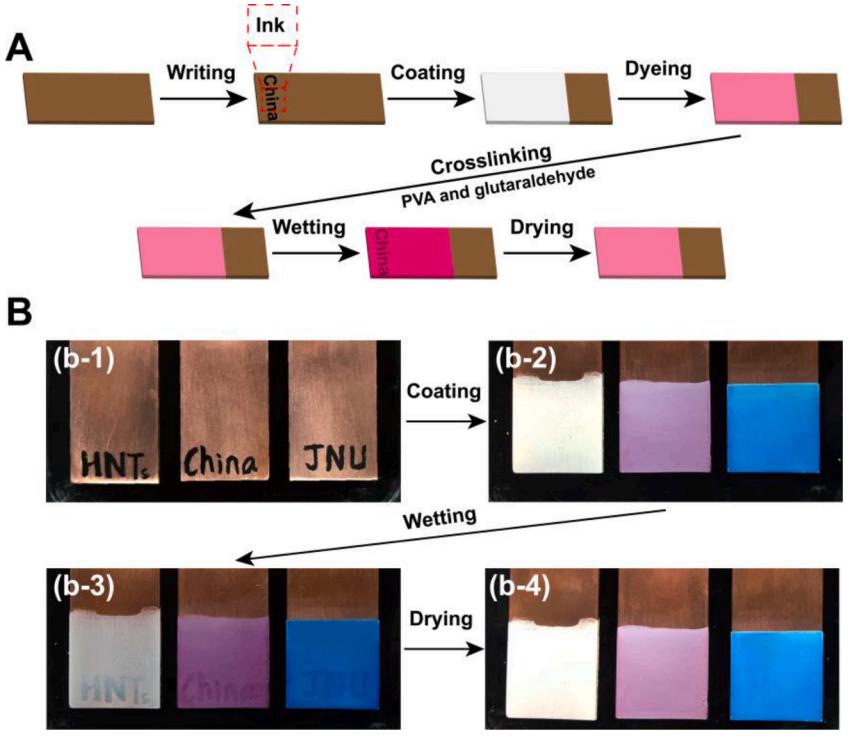

Fig. 7. Application of HNTs/PVA composite coating for information hiding. Schematic showing the preparation of HNTs/PVA composite coatings that can be information-hiding (A); photos of a typical HNTs/PVA composite coating used for information-hiding (B).

designed, as shown in Fig. 8**B**. Using 2.5% $FeCl_3$ as the etching solution [54], copper rods and copper rods with the HNTs/PVA composite coating were placed in the etching solution, and the integrity of the coating was observed. In terms of coating integrity, the coating integrity was increasingly good for deposition times of 15 s to 60 s. The corrosion resistance of the HNTs/PVA composite coating increased with increasing coating thickness within a specific range.

To further investigate the corrosion resistance of the HNTs/PVA composite coating, the corrosion reaction kinetics of the anodes with different coating thicknesses were analyzed using electrochemical impedance spectroscopy (EIS). A three-electrode system was used [55] . The copper rod with HNTs/PVA composite coating as the working electrode, and the counter and reference electrodes are a graphite electrode and a standard glycerol electrode (SCE), respectively. The AC impedance profiles at open circuit potential in 2.5% NaCl electrolyte.

The EIS results are shown in Fig. 8**C.**The semicircle in the mid-frequency band is related to the electrochemical reaction impedance. At the same time, the diagonal line in the low-frequency region is related to the solid-state ion diffusion in the electrode body [56]. The semicircle diameter of the HTNs/PVA composite coating in Fig. 8C with an EPD time of 15, 30, 45 and 60 s is about 19,000, 23,870, 29,300, and 33,560, respectively. The longer the EPD time, the larger the semicircle radius. The semicircle diameter of the copper rod is much smaller than the semicircle diameter of the copper coated with the HNTs/PVA composite coating. As the smaller diameter of the semicircle diameter indicates a lower charge transfer impedance, the corresponding corrosion current is higher. Therefore, the large semicircle diameter of the HNTs/PVA composite coating suggests improved corrosion resistance.

The EIS data was fitted by the equivalent circuit diagram as shown in Fig. 8**D**. The EIS fitting parameters are listed in the Table 1. R_Ω is the

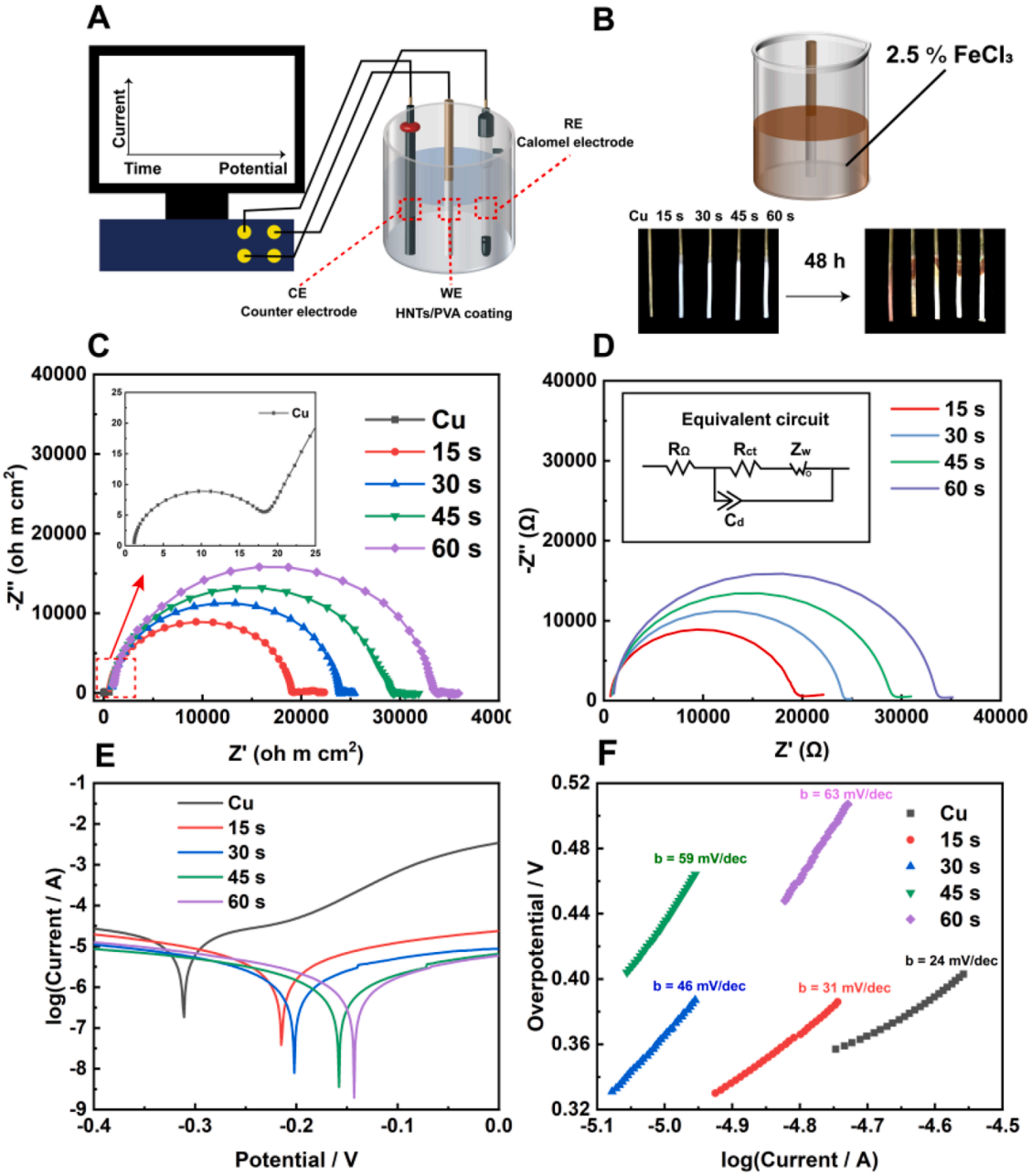

Fig. 8. Study of corrosion resistance of HNTs/PVA composite coatings with EPD time of 15 s-60 s. Schematic showing the process of electrochemical resistance test (A); protective effect of the coating in $FeCl_3$ solution (B); EIS test result of HNTs/PVA composite coated Cu rod and raw Cu rod (C); The EIS curve fits and equivalent circuits for deposition time of 15–60 s (D); polarization curves (E); Tafel slope (F) of the Cu and Cu with different HNTs/PVA composite coatings.

Table 1
EIS parameters obtained by fitting according to the equivalent circuit diagram.

Time (s)	15	30	45	60
R_Ω (Ω cm^2)	648.1	786.7	862.1	994.2
R_{ct} (Ω cm^2)	13,446.0	14,729.0	22,632.0	27,015.0
Z_w (Ω cm^2 $s^{-1/2}$)	6345.0	7706.0	7303.0	6795.0
C_d (F cm^{-2})	2.9×10^{-9}	2.7×10^{-9}	2.2×10^{-9}	1.8×10^{-9}

electrolyte resistance, R_{ct} is the coating resistance, Z_w and C_d denote the Warburg diffusion impedance and capacitance, respectively [57,58]. From the EIS parameters, it can be seen that the coating resistance increases with the increase of deposition time. When the deposition time increased from 15 to 60 s, the coating resistance changed from 13,446.0 to 27,015.0 Ω cm^2. All these confirmed the increased anti-corrosion ability by the HNTs coatings.

In addition, the time-dependent trend of the EIS plot of the HNT coated Cu rod was also explored, as shown in Fig. S3. The resistance of initial HNTs coated Cu (0 h) was the smallest (about 60,000 Ω). The resistance of 12 h soaking with 2.5% NaCl solution is the largest, about 130,000 Ω. When soaking for 24 and 48 h, the resistance decreases to about 100,000 and 85,000 Ω, respectively. All these values were larger than that of the raw Cu. When the soaking time was less than 12 h, the copper was partly corroded, leading to an increase in resistance. Then, the damage of the HNTs coating at 12–48 h leaded to a decrease in resistance.

Tafel plots and Tafel slope plots were also measured. Electrochemical parameters related to polarization measurements, such as corrosion potential (E_{corr}), corrosion current density (j_{corr}), polarization resistance (R_p), and Tafel slopes (β_c and β_a), are listed in Table 2. It can be seen that the E_{corr} shifts from −215 to −143 mV when the deposition time increases from 15 to 60 s. In addition, the value of j_{corr} decreases as the electrophoretic deposition time increases. Therefore, the thicker the coating of HNTs in the appropriate range, the better the corrosion resistance [58]. Extended EPD time increases the absolute value of the corrosion potential. The absolute values of the corrosion potentials increase in the following order. Copper < 15 *s* < 30 *s* < 45 *s* < 60 s. The larger the absolute value of the corrosion potential, the better the corrosion resistance [59]. The Tafel slope graph Fig. 8**F** shows that the Tafel slope increases in the following order: Cu < 15 *s* < 30 *s* < 45 *s* < 60 s. The principle of the Tafel slope shows that the larger the slope, the smaller the electron transfer rate, the slower the reaction rate, and the more complex the reaction occur. Hence, the resistance to oxidation and corrosion is stronger in composite coatings. In conclusion, HNTs/PVA coating can substantially improve the corrosion resistance of metals, and the thicker the coating, the better the corrosion resistance. The HNTs/PVA composite coating has a great potential application in metal protection.

4. Conclusions

A fast, low-cost, and facial protection method for metals was proposed to improve the service life of metallic materials and equipment by EPD of HNTs coatings. The thickness and weight of the coating can be precisely controlled by varying the conditions of the electrophoretic deposition. PVA crosslinked with GA was further introduced into HNTs coating for improving corrosion resistance, wear resistance, and water resistance. The experiments explored the application of HNTs/PVA composite coatings on metals, including thermal insulation, information hiding, and corrosion protection. This work develops a method to assemble tubular nanoclay on metal substrates by EPD and polymer modification, which shows excellent potential in metal corrosion protection.

Table 2
Tafel parameters of HNTs coatings in 2.5% NaCl solution.

Time (s)	15	30	45	60
$\mathbf{E}_{corr}$ (mV)	−215	−157	−152	−143
$\boldsymbol{\beta}_c$ (mV dec^{-1})	4.92	5.02	4.99	5.07
$\boldsymbol{\beta}_a$ (mV dec^{-1})	4.99	5.11	6.83	5.28
$\mathbf{R}_P$ (Ω cm^2)	9590.9	21,296.1	28,736.6	25,002.7
$\mathbf{j}_{corr}$ (mA cm^{-2})	1.017	0.3875	0.2207	0.2196

CRediT authorship contribution statement

Yao Wang: Investigation, Data curation, Writing – original draft. **Yuer Yang:** Investigation, Methodology, Validation. **Mingxian Liu:** Funding acquisition, Project administration, Writing – review & editing.

Declaration of Competing Interest

The authors declare that they have no known competing financial interests or personal relationships that could have appeared to influence the work reported in this paper.

Acknowledgments

This work was financially supported by the National Natural Science Foundation of China (52073121), the Natural Science Foundation of Guangdong Province (2019A1515011509), the Science and Technology Program of Guangzhou (202102010117), and the Fundamental Research Funds for the Central Universities (21622406).

Data availability

The raw/processed data required to reproduce these findings cannot be shared at this time due to legal or ethical reasons.

Supplementary materials

Supplementary material associated with this article can be found, in the online version, at doi:10.1016/j.apmt.2022.101657.

References

[1] H. Wei, Y. Wang, J. Guo, N.Z. Shen, D. Jiang, X. Zhang, X. Yan, J. Zhu, Q. Wang, L. Shao, Advanced micro/nanocapsules for self-healing smart anticorrosion coatings, J. Mater. Chem. A 3 (2) (2015) 469–480.
[2] H. Wang, J. Xu, X. Du, Z. Du, X. Cheng, H. Wang, A self-healing polyurethane-based composite coating with high strength and anti-corrosion properties for metal protection, Compos. B. Eng. 225 (2021), 109273.
[3] N. Eliaz, Corrosion of metallic biomaterials: a review, Materials (Basel) 12 (3) (2019) 407.
[4] G. Grundmeier, W. Schmidt, M. Stratmann, Corrosion protection by organic coatings: electrochemical mechanism and novel methods of investigation, Electrochim. Acta 45 (15–16) (2000) 2515–2533.
[5] L. Ma, C. Ren, J. Wang, T. Liu, H. Yang, Y. Wang, Y. Huang, D. Zhang, Self-reporting coatings for autonomous detection of coating damage and metal corrosion: a review, Chem. Eng. J. 421 (2021), 127854.
[6] Y. Ma, H. Huang, H. Zhou, M. Graham, J. Smith, X. Sheng, Y. Chen, L. Zhang, X. Zhang, E. Shchukina, D. Shchukin, Superior anti-corrosion and self-healing bi-functional polymer composite coatings with polydopamine modified mesoporous silica/graphene oxide, J. Mater. Sci. Technol. 95 (2021) 95–104.
[7] V.S. Saji, Advanced corrosion prevention approaches: smart coating and photoelectrochemical cathodic protection,. Corrosion and Fouling Control in Desalination Industry, Springer, 2020, pp. 225–247.
[8] K.A. Zahidah, S. Kakooei, M.C. Ismail, P.B. Raja, Halloysite nanotubes as nanocontainer for smart coating application: a review, Prog. Org. Coat. 111 (2017) 175–185.
[9] X. He, S. Li, R. Shen, Y. Ma, L. Zhang, X. Sheng, Y. Chen, D. Xie, J. Huang, A high-performance waterborne polymeric composite coating with long-term anti-corrosive property based on phosphorylation of chitosan-functionalized Ti3C2Tx MXene, Adv. Compos. Hybrid Mater. 5 (2022) 1699–1711.
[10] I. Deen, I. Zhitomirsky, Electrophoretic deposition of composite halloysite nanotube–hydroxyapatite–hyaluronic acid films, J. Alloy. Compd. 586 (2014) S531–S534.

[11] J. Li, I. Zhitomirsky, Cathodic electrophoretic deposition of manganese dioxide films, Colloids Surf. Physicochem. Eng. Asp. 348 (1–3) (2009) 248–253.
[12] M. Cheong, I. Zhitomirsky, Electrodeposition of alginic acid and composite films, Colloids Surf. Physicochem. Eng. Asp. 328 (1–3) (2008) 73–78.
[13] Y. Li, K. Wu, I. Zhitomirsky, Electrodeposition of composite zinc oxide–chitosan films, Colloids Surf. Physicochem. Eng. Asp. 356 (1–3) (2010) 63–70.
[14] M. Diba, D.W. Fam, A.R. Boccaccini, M.S. Shaffer, Electrophoretic deposition of graphene-related materials: a review of the fundamentals, Prog. Mater. Sci. 82 (2016) 83–117.
[15] L. Besra, M. Liu, A review on fundamentals and applications of electrophoretic deposition (EPD), Prog. Mater. Sci 52 (1) (2007) 1–61.
[16] L. Shao, X. Wang, B. Yang, Q. Wang, Q. Tian, Z. Ji, J. Zhang, A highly sensitive ascorbic acid sensor based on hierarchical polyaniline coated halloysite nanotubes prepared by electrophoretic deposition, Electrochim. Acta 255 (2017) 286–297.
[17] S.A. Hasan, D.W. Kavich, S.V. Mahajan, J.H. Dickerson, Electrophoretic deposition of CdSe nanocrystal films onto dielectric polymer thin films, Thin Solid Films 517 (8) (2009) 2665–2669.
[18] A.R. Boccaccini, J. Cho, J.A. Roether, B.J. Thomas, E.J. Minay, M.S. Shaffer, Electrophoretic deposition of carbon nanotubes, Carbon N Y 44 (15) (2006) 3149–3160.
[19] D. Marcin Behunová, G. Gallios, V. Girman, H. Kolev, M. Kaňuchová, S. Dolinská, M. Václavíková, Electrophoretic deposition of graphene oxide on stainless steel substrate, Nanomaterials 11 (7) (2021) 1779.
[20] M.J. Hwang, M.G. Kim, S. Kim, Y.C. Kim, H.W. Seo, J.K. Cho, I.K. Park, J. Suhr, H. Moon, J.C. Koo, Cathodic electrophoretic deposition (EPD) of phenylenediamine-modified graphene oxide (GO) for anti-corrosion protection of metal surfaces, Carbon N Y 142 (2019) 68–77.
[21] B. Thomas, A. Boccaccini, M. Shaffer, Multi-walled carbon nanotube coatings using electrophoretic deposition (EPD), J. Am. Ceram. Soc. 88 (4) (2005) 980–982.
[22] P. Yuan, D. Tan, F. Annabi-Bergaya, W. Yan, D. Liu, Z. Liu, From platy kaolinite to aluminosilicate nanoroll via one-step delamination of kaolinite: effect of the temperature of intercalation, Appl. Clay Sci. 83 (2013) 68–76.
[23] M. Liu, Z. Jia, D. Jia, C. Zhou, Recent advance in research on halloysite nanotubes-polymer nanocomposite, Prog. Polym. Sci. 39 (8) (2014) 1498–1525.
[24] Y. Zhang, Y. Chen, H. Zhang, B. Zhang, J. Liu, Potent antibacterial activity of a novel silver nanoparticle-halloysite nanotube nanocomposite powder, J. Inorg. Biochem. 118 (2013) 59–64.
[25] K. Hedicke-Höchstötter, G.T. Lim, V. Altstädt, Novel polyamide nanocomposites based on silicate nanotubes of the mineral halloysite, Compos. Sci. Technol. 69 (3–4) (2009) 330–334.
[26] M. Liu, C. Wu, Y. Jiao, S. Xiong, C. Zhou, Chitosan–halloysite nanotubes nanocomposite scaffolds for tissue engineering, J. Mater. Chem. B 1 (15) (2013) 2078–2089.
[27] R. Kamble, M. Ghag, S. Gaikawad, B.K. Panda, Halloysite nanotubes and applications: a review, J. Adv. Res. 3 (2) (2012).
[28] Y.M. Lvov, D.G. Shchukin, H. Mohwald, R.R. Price, Halloysite clay nanotubes for controlled release of protective agents, ACS Nano 2 (5) (2008) 814–820.
[29] Y.P. Wu, J. Yang, H.Y. Gao, Y. Shen, L. Jiang, C. Zhou, Y.F. Li, R.R. He, M. Liu, Folate-conjugated halloysite nanotubes, an efficient drug carrier, deliver doxorubicin for targeted therapy of breast cancer, ACS Appl. Nano Mater. 1 (2) (2018) 595–608.
[30] G. Wang, X. Chen, S. Liu, C. Wong, S. Chu, Mechanical chameleon through dynamic real-time plasmonic tuning, ACS Nano 10 (2) (2016) 1788–1794.
[31] Y. Yang, Y. Chen, F. Leng, L. Huang, Z. Wang, W. Tian, Recent advances on surface modification of halloysite nanotubes for multifunctional applications, Appl. Sci. 7 (12) (2017) 1215.
[32] Y. Wang, I. Deen, I. Zhitomirsky, Electrophoretic deposition of polyacrylic acid and composite films containing nanotubes and oxide particles, J. Colloid Interface Sci. 362 (2) (2011) 367–374.
[33] S.B.A. Boraei, J. Nourmohammadi, F.S. Mahdavi, J. Yus, A. Ferrandez-Montero, A. J. Sanchez-Herencia, Z. Gonzalez, B. Ferrari, Effect of SrR delivery in the biomarkers of bone regeneration during the *in vitro* degradation of HNT/GN coatings prepared by EPD, Colloids Surf. B. Biointerfaces 190 (2020), 110944.
[34] T. Yu, Z. Chen, S.-.J. Park, Y.-.H. Kim, Electrophoresis deposited halloysite nanotubes as modifying additive for carbon fiber and CFRP, Mod. Phys. Lett. B 33 (14n15) (2019), 1940023.
[35] A. Humayun, Y. Luo, D.K. Mills, Electrophoretic deposition of gentamicin-loaded znhnts-chitosan on titanium, Coatings 10 (10) (2020) 944.
[36] N.S. Jackoub Raddaha, S. Seuss, A.R. Boccaccini, Study of the electrophoretic deposition of chitosan/halloysite nanotubes/titanium dioxide composite coatings using Taguchi experimental design approach, Key Eng. Mater. (2015) 230–239.
[37] N.S. Radda'a, W.H. Goldmann, R. Detsch, J.A. Roether, L. Cordero-Arias, S. Virtanen, T. Moskalewicz, A.R. Boccaccini, Electrophoretic deposition of tetracycline hydrochloride loaded halloysite nanotubes chitosan/bioactive glass composite coatings for orthopedic implants, Surf. Coat. Technol. 327 (2017) 146–157.
[38] M. Farrokhi-Rad, M. Mohammadalipour, T. Shahrabi, Removal of methylene blue from aqueous solution by electrophoretically deposited titania-halloysite nanotubes coatings, J. Am. Ceram. Soc. 101 (11) (2018) 4942–4955.
[39] A. Molaei, A. Amadeh, M. Yari, M.R. Afshar, Structure, apatite inducing ability, and corrosion behavior of chitosan/halloysite nanotube coatings prepared by electrophoretic deposition on titanium substrate, Mater. Sci. Eng. C 59 (2016) 740–747.
[40] M. Farrokhi-Rad, A. Fateh, T. Shahrabi, Electrophoretic deposition of vancomycin loaded halloysite nanotubes-chitosan nanocomposite coatings, Surf. Coat. Technol. 349 (2018) 144–156.
[41] T. Yu, Z. Chen, S.-.J. Park, Y.-.H. Kim, Electrophoretic deposition of non-conductive halloysite nanotubes onto glass fabrics with improved interlaminar properties of glass/epoxy composites, Int. J. Mod. Phys. B 35 (14n16) (2021), 2140033.
[42] D. Tan, P. Yuan, D. Liu, P. Du, Surface Modifications of halloysite, Developments in Clay Science, Elsevier, 2016, pp. 167–201.
[43] M. Liu, R. Fakhrullin, A. Novikov, A. Panchal, Y. Lvov, Tubule nanoclay-organic heterostructures for biomedical applications, Macromol. Biosci. 19 (4) (2019), 1800419.
[44] Y. Wang, Y.L. Hsieh, Crosslinking of polyvinyl alcohol (PVA) fibrous membranes with glutaraldehyde and PEG diacylchloride, J. Appl. Polym. Sci. 116 (6) (2010) 3249–3255.
[45] M. Ghanbari, D. Emadzadeh, W. Lau, T. Matsuura, A. Ismail, Synthesis and characterization of novel thin film nanocomposite reverse osmosis membranes with improved organic fouling properties for water desalination, RSC Adv. 5 (27) (2015) 21268–21276.
[46] Y. Lvov, A. Panchal, Y. Fu, R. Fakhrullin, M. Kryuchkova, S. Batasheva, A. Stavitskaya, A. Glotov, V. Vinokurov, Interfacial self-assembly in halloysite nanotube composites, Langmuir 35 (26) (2019) 8646–8657.
[47] M. Liu, B. Guo, M. Du, D. Jia, Drying induced aggregation of halloysite nanotubes in polyvinyl alcohol/halloysite nanotubes solution and its effect on properties of composite film, Appl. Phys. A 88 (2) (2007) 391–395.
[48] P. Yuan, P.D. Southon, Z. Liu, M.E. Green, J.M. Hook, S.J. Antill, C.J. Kepert, Functionalization of halloysite clay nanotubes by grafting with γ-aminopropyltriethoxysilane, J. Phys. Chem. C 112 (40) (2008) 15742–15751.
[49] A. Jones, Ball motion and sliding friction in ball bearings, J. Basic. Eng. 81 (1) (1959) 1–12.
[50] G. Zeng, Y. He, Y. Zhan, L. Zhang, Y. Pan, C. Zhang, Z. Yu, Novel polyvinylidene fluoride nanofiltration membrane blended with functionalized halloysite nanotubes for dye and heavy metal ions removal, J. Hazard. Mater. 317 (2016) 60–72.
[51] D.Y. Yang, C.P. Hu, S.K. Ying, Preparation and characterization of waterborne poly (urethane urea) with well-defined hard segments, J. Polym. Sci. Part A Polym. Chem. 43 (12) (2005) 2606–2614.
[52] H. Vedala, J. Huang, X.Y. Zhou, G. Kim, S. Roy, W.B. Choi, Effect of PVA functionalization on hydrophilicity of Y-junction single wall carbon nanotubes, Appl. Surf. Sci. 252 (22) (2006) 7987–7992.
[53] R.P. Shaikh, P. Kumar, Y.E. Choonara, L.C. Du Toit, V. Pillay, Crosslinked electrospun PVA nanofibrous membranes: elucidation of their physicochemical, physicomechanical and molecular disposition, Biofabrication 4 (2) (2012), 025002.
[54] O. Sisso, S. Dor, D. Eliyahu, E. Sabatani, N. Eliaz, Corrosion inhibition of copper in ferric chloride solutions with organic inhibitors, npj Mater. Degrad. 4 (1) (2020) 1–16.
[55] S.H. Yang, C.Y. Chen, W.J. Wang, An impedance study for the anode micro-porous layer in an operating direct methanol fuel cell, J. Power Sources 195 (11) (2010) 3536–3545.
[56] H. Liu, H. Guo, B. Liu, M. Liang, Z. Lv, K.R. Adair, X. Sun, Few-layer MoSe2 nanosheets with expanded (002) planes confined in hollow carbon nanospheres for ultrahigh-performance Na-ion batteries, Adv. Funct. Mater. 28 (19) (2018), 1707480.
[57] K.V. Subramaniam, M. Bi, Investigation of steel corrosion in cracked concrete: evaluation of macrocell and microcell rates using Tafel polarization response, Corros Sci 52 (8) (2010) 2725–2735.
[58] M.A. Amin, K.F. Khaled, S.A. Fadl-Allah, Testing validity of the Tafel extrapolation method for monitoring corrosion of cold rolled steel in HCl solutions – Experimental and theoretical studies, Corros. Sci. 52 (1) (2010) 140–151.